Orai-STIM–mediated Ca^{2+} release from secretory granules revealed by a targeted Ca^{2+} and pH probe

Eamonn J. Dickson[a,1], Joseph G. Duman[a,1,2], Mark W. Moody[a], Liangyi Chen[b], and Bertil Hille[a,3]

[a]Department of Physiology and Biophysics, University of Washington School of Medicine, Seattle, WA 98195; and [b]Institute of Molecular Medicine, Peking University, Beijing 100871, People's Republic of China

Contributed by Bertil Hille, October 18, 2012 (sent for review October 1, 2012)

Secretory granules (SGs) sequester significant calcium. Understanding roles for this calcium and potential mechanisms of release is hampered by the difficulty of measuring SG calcium directly in living cells. We adapted the Förster resonance energy transfer-based D1-endoplasmic reticulum (ER) probe to develop a unique probe (D1-SG) to measure calcium and pH in secretory granules. It significantly localizes to SGs and reports resting free Ca^{2+} of 69 ± 15 μM and a pH of 5.8. Application of extracellular ATP to activate P2Y receptors resulted in a slow monotonic decrease in SG Ca^{2+} temporally correlated with the occurrence of store-operated calcium entry (SOCE). Further investigation revealed a unique receptor-mediated mechanism of calcium release from SGs that involves SG store-operated Orai channels activated by their regulator stromal interaction molecule 1 (STIM1) on the ER. SG Ca^{2+} release is completely antagonized by a SOCE antagonist, by switching to Ca^{2+}-free medium, and by overexpression of a dominant-negative Orai1(E106A). Overexpression of the CRAC activation domain (CAD) of STIM1 resulted in a decrease of resting SG Ca^{2+} by ∼75% and completely abolished the ATP-mediated release of Ca^{2+} from SGs. Overexpression of a dominant-negative CAD construct (CAD-A376K) induced no significant changes in SG Ca^{2+}. Colocalization analysis suggests that, like the plasma membrane, SG membranes also possess Orai1 channels and that during SG Ca^{2+} release, colocalization between SGs and STIM1 increases. We propose Orai channel opening on SG membranes as a potential mode of calcium release from SGs that may serve to raise local cytoplasmic calcium concentrations and aid in refilling intracellular calcium stores of the ER and exocytosis.

SERCA | cameleon | FRET | purinergic | IP_3

Here, we consider the Ca^{2+} dynamics of secretory compartments and describe a unique mechanism of Ca^{2+} release from them. Cells maintain cytoplasmic Ca^{2+} at nanomolar concentrations but elevate it locally in response to many signals. Elevated cytoplasmic Ca^{2+} modulates the functions of signaling cascades and enzymes, regulating many cellular responses (1). Two major sources feed most known cytoplasmic Ca^{2+} elevations: the extracellular space and the endoplasmic reticulum (ER). Here, we are interested in an additional intracellular source of Ca^{2+}.

Like the ER, secretory granules (SGs) contain a lot of Ca^{2+}. They bud from the trans-Golgi network, and during subsequent maturation, they acquire an intraluminal pH of 5.5–5.9 (2), electron-dense cores (3), and matrices that bind Ca^{2+} and other ions (4). Their cargo is destined for release by regulated exocytosis, often triggered by Ca^{2+} signals. Only a small fraction of SGs undergo exocytosis after a given stimulus and are then typically recovered by endocytosis (5–7). Total Ca^{2+} in SGs is remarkably high, at 30–40 mM (8, 9). The free Ca^{2+} is significantly lower, with estimates ranging from 10 to 80 μM (10–14), which is still well above that in the cytoplasm. Roles for granular Ca^{2+} remain to be understood.

There is no clear picture of SG Ca^{2+} dynamics. Ca^{2+} may be captured while SG Ca^{2+} buffers transit through the secretory pathway starting with the ER, and Ca^{2+}could be imported continually into mature SGs. Several mechanisms for Ca^{2+} import have been proposed, including Ca^{2+}-transporting ATPases, such as "secretory pathway Ca^{2+} ATPase," cotransport using the proton gradient across the SG, and Na^+/Ca^{2+} exchange secondarily driven by H^+/Na^+ exchange (11, 15, 16). Contributing to the uncertainties in this field has been the difficulty in measuring SG Ca^{2+} directly in living cells. Low-affinity chemical Ca^{2+} probes, such as mag-fura, can measure free Ca^{2+} at granular levels and at acidic pH (10) but are limited by the difficulty in ensuring that the signals originate from the compartment of interest. Genetically targeted granular Ca^{2+} probes based on the photoprotein aequorin have been developed that have the proper Ca^{2+} affinity, pH insensitivity, and subcellular localization (11, 12), but they are consumed after releasing one photon, such that thousands of cells must be measured in suspension to have sufficient signal and imaging is precluded.

Store-operated calcium entry (SOCE) is a process in which depletion of calcium stores in the ER induces calcium influx from the extracellular space (17). Stimulation of plasma membrane receptors coupled to G_q activates phospholipase C, generating inositol trisphosphate (IP_3); IP_3 releases Ca^{2+} from the ER and raises cytoplasmic Ca^{2+}. Eventually, stromal interaction molecules (STIMs) in the ER membrane sense ER Ca^{2+} depletion, oligomerize, and become active. They aggregate in the ER membrane just under the plasma membrane, promoting clustering and activation of Orai1 channels on the plasma membrane, initiating SOCE in membrane patches (18–20). Local Ca^{2+} entry there raises the submembrane Ca^{2+} concentration, promoting an adaptive partial inactivation of SOCE (21) and loosening the STIM–Orai interaction (22, 23). Eventual refilling of the ER gradually reverses the activation of STIM1.

We now describe the development and use of a cameleon probe for monitoring Ca^{2+} and pH in SGs. Like the aequorin-based probes, it is genetically targeted to SGs, and like other

Significance

Elevated cytoplasmic calcium modulates many cellular responses. Two Ca^{2+} sources feed most cytoplasmic Ca^{2+} elevations, the extracellular space and the endoplasmic reticulum. We found that secretory granules represent another Ca^{2+} source that releases Ca^{2+} in a physiologically interesting way. We developed a targeted probe for monitoring Ca^{2+} in secretory granules. It revealed a unique receptor-stimulated mechanism of Ca^{2+} release from secretory granules apparently involving "store-operated" Orai channels in the secretory granule membrane. The channels open when reticular stores are depleted. Such Ca^{2+} release from granules might elevate local Ca^{2+} concentrations and aid in the refilling of other cytoplasmic Ca^{2+} stores.

Author contributions: E.J.D., J.G.D., L.C., and B.H. designed research; E.J.D., J.G.D., M.W.M., and L.C. performed research; E.J.D., J.G.D., M.W.M., and L.C. analyzed data; and E.J.D., J.G.D., L.C., and B.H. wrote the paper.

The authors declare no conflict of interest.

[1]E.J.D. and J.G.D. contributed equally to this work.

[2]Present address: Department of Neuroscience, Baylor College of Medicine, Houston, TX 77030.

[3]To whom correspondence should be addressed. E-mail: hille@u.washington.edu.

This article contains supporting information online at www.pnas.org/lookup/suppl/doi:10.1073/pnas.1218247109/-/DCSupplemental.

cameleons, it is based on Förster resonance energy transfer (FRET) and is usable for subcellular imaging with single cells. With this tool, we discovered a unique mechanism of Ca^{2+} release from SGs apparently involving Orai channels in the SG membrane. This mode of calcium release from SGs might elevate local Ca^{2+} concentrations and aid in the refilling of other cytoplasmic Ca^{2+} stores.

Results

Calcium Sensitivity of a Cameleon Probe at Low pH. We developed a genetically expressible probe to measure Ca^{2+} in SGs. A suitable probe must be (*i*) able to measure and report Ca^{2+} in the acidic pH range of secretory compartments and (*ii*) localized within SGs. This section concerns the first criterion, appropriate measurement sensitivity. As a building block, we started with D1-ER, an ER-targeted cameleon-like probe (24) (Fig. 1*A*). It contains a low-affinity Ca^{2+} sensor based on Ca^{2+}-dependent binding of a modified calmodulin (CaM) with a modified CaM-binding peptide (M13) from myosin light-chain kinase. The sensor domain is flanked by cyan fluorescent protein (CFP) and citrine, functioning as a FRET reporter pair. Calcium binding to the sensor increases their FRET interaction. D1-ER has a broad range of Ca^{2+} sensitivity over the expected values of SG Ca^{2+} thanks to its two binding affinities for Ca^{2+} [K_ds for Ca^{2+} of 0.81 μM and 60 μM (24)].

We tested the ability of D1-ER to measure Ca^{2+} under acidic pH conditions by expressing it in PC12 cells, where it localizes in the ER together with many proteins destined for SGs. For calibrations, cell membranes were permeabilized with digitonin and the bath pH and Ca^{2+} were buffered in the presence of the ionophores ionomycin and monensin. Once cells were permeabilized and equilibrated, we measured FRET ratio (FRETr) values from a probe in the ER. As described in *Materials and Methods* and *SI Materials and Methods*, photometric measurements were made on single cells of corrected fluorescence from CFP (CFP_C) and YFP (YFP_C) in response to excitation of CFP. The subscript "C" denotes excitation with CFP wavelength, and YFP denotes that citrine emission is recorded at a conventional YFP emission wavelength. The FRETr was defined as YFP_C/CFP_C. D1-ER responded to free Ca^{2+} over a range of 10 μM to 5 mM at pH values ranging from 5.5 to 7.4 (Fig. 1*B*). These calibration curves varied with the pH in a graded manner. Thus, D1-ER responds to Ca^{2+} at the expected SG pH values, but simultaneous knowledge of the SG pH is necessary to interpret FRET measurements as calibrated free-Ca^{2+} values. In *Materials and Methods* and *SI Materials and Methods* (Fig. S1*A*), we develop empirical formulas that calculate [Ca^{2+}], given the observed FRET and pH.

Targeting the Probe. The second requirement was to direct the probe to SGs. We removed the ER signal sequence and the ER retention motif from D1-ER and tested several granular protein sequences for their ability to direct the probe to granules. Attempts to use neuropeptide Y and phogrin were unsuccessful, but when fused to tissue plasminogen activator (tPA) (Fig. 1*A*), the probe assumed a granular appearance 3 d after transient transfection into PC12 cells. We named the newly developed probe D1-SG and now characterize its localization in detail. Fig. 1*C* shows representative confocal images from PC12 cells transfected with D1-SG, fixed 3 d later, and stained with antibodies against markers of cellular compartments. To test for colocalization of our probe with individual markers, we used several methods. Pearson's correlation analysis cross-correlates image pairs on a pixel-by-pixel basis, and a unique type of analysis, detailed in *Materials and Methods* and Fig. S2, computes distances between multipixel puncta ("granular objects") of one protein and multipixel puncta of another. Such analyses are not sensitive to the relative intensities of the probe and organellar markers. There was strong overlap (correlation) with the SG marker chromogranin B (CgB), although not all CgB-positive

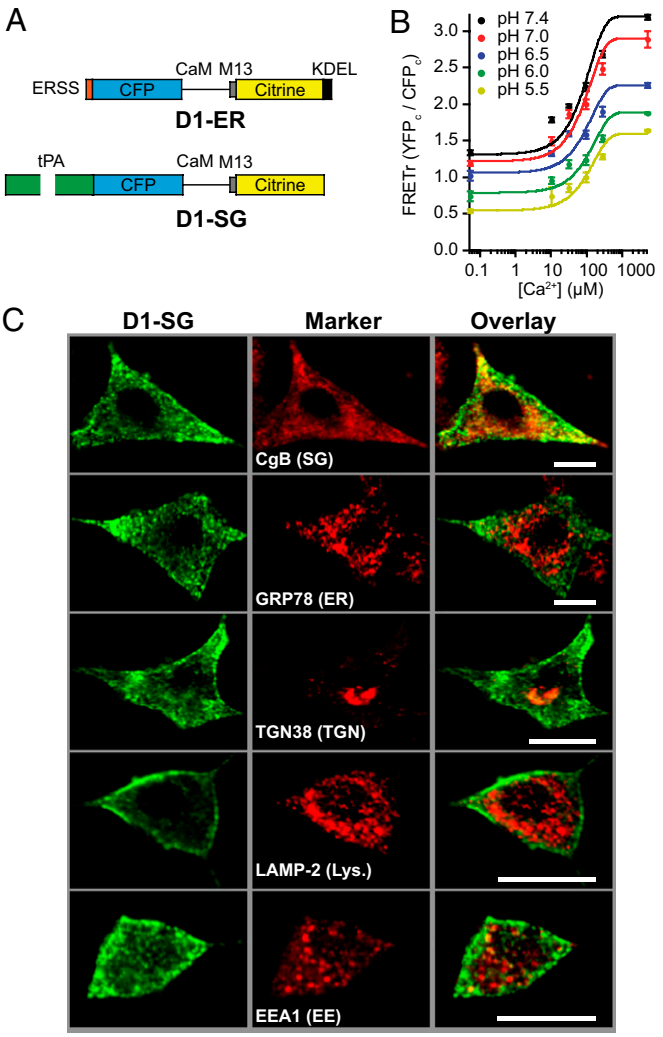

Fig. 1. Design, calibration, and localization of D1-SG. (*A*) Schematic of the D1-ER and D1-SG cameleons drawn approximately to scale. CaM, mutant calmodulin; CFP, enhanced cyan fluorescent protein; ERSS, ER signal sequence; KDEL, KDEL ER retention motif; M13, mutant skeletal muscle myosin light-chain kinase peptide. (*B*) FRETr responses to known free [Ca^{2+}] solutions at pH values ranging from 5.5 to 7.4 in permeabilized PC12 cells transiently transfected with the D1-ER probe. Mean ± SEM values (n = 20 for each point) are shown. The fitted empirical curves are solutions of Eq. **1** with coefficients given in Fig. S1. (*C*) Representative confocal images from PC12 cells expressing D1-SG (green, *Left*) fixed and immunostained for protein markers of various cellular organelles (red, *Center*). (*Right*) Red and green images are merged. Images are representative of seven confocal images from three different preparations. Lys., lysosomes. EE, early endosomes. (Scale bars: 10 μm.)

structures had D1-SG fluorescence (Table 1). This may suggest different populations of granules that differ in as simple a parameter as whether they were formed during the window of probe expression, because mature SGs are not likely to accept new incoming cargo from the Golgi. Two other markers, early endosome antigen 1 (EEA1) and lysosome-associated membrane protein 2 (LAMP-2; lysosomes), showed weaker potential overlap with D1-SG using the Pearson method and the more sensitive puncta-based method (Table 1 and Fig. S2). An analysis of line scans given in Fig. S3 also showed minor overlap with these two probes at 3 d. Our probe showed no significant overlap with markers for the ER (GRP78), Golgi apparatus (GM130), trans-Golgi network (TGN38), or mitochondria (Mcl-1). We interpret these observations as meaning that the majority of D1-SG is localized to SGs.

Table 1. Tests of colocalization with D1-SG

Organelle marker and (organelle)	Pixel correlation, $r_{pearson}$	% overlap granular objects	*P*
CgB (SG)	0.53 ± 0.1	54 ± 1	—
GRP78 (ER)	0.30 ± 0.1	—	—
GM130 (Golgi)	0.15 ± 0.1	—	—
TGN38 (TGN)	0.16 ± 0.1	—	—
EEA1 (EE)	0.44 ± 0.1	14 ± 1	<0.001
LAMP-2 (lysosomes)	0.36 ± 0.1	18 ± 1	<0.05
Mcl-1 (mitochondria)	0.30 ± 0.1	—	—

% overlap is the percentage of D1-SG granular objects within the criterion distance of identified organelle marker granular objects. $r_{pearson}$, Pearson correlation coefficient between D1-SG pixels and "marker" pixels.

Measuring pH with the Probe. The next step was to establish a means to measure pH during granular Ca^{2+} measurements. We did this primarily to be able to interpret the FRET measurements as calibrated free-Ca^{2+} values; however, following SG pH in real time is of interest in its own right. As for most fluorescent proteins, the fluorescence of the citrine fluorophore is quenched by protonation at low pH. We reasoned that if we directly excited the enhanced CFP and citrine fluorophores sequentially, we could read the FRETr (for Ca^{2+}) from CFP_C and YFP_C during the CFP excitation and measure pH using citrine emission (YFP_Y) during direct citrine excitation. The pH measurement is a single-wavelength measurement that requires the unquenched high-pH maximum fluorescence value of YFP_Y to convert the fluorescence intensity readings to pH. The maximum value was found by deprotonating the citrine at the end of each experiment with alkaline ammonium chloride. Applying a pH 7.5 solution of NH_4Cl (20 mM) to the exterior of an intact cell expressing granule-targeted fluorescent protein rapidly increased the YFP_Y fluorescence (Fig. 2*A*). Shifting to pH 8.5 maximally dequenched the fluorophore, and increasing the concentration of NH_4Cl to 50 mM gave no further change. Therefore, at the end of the experiments, a 20-mM NH_4Cl solution with a pH of 8.0 or 8.5 was applied to determine the maximum YFP_Y fluorescence. In calibration experiments with permeabilized cells, we created a standard pH titration curve for citrine (Fig. 2*B*). From this curve, the apparent pK_a of citrine is 5.8, similar to the reported value of 5.7 (24, 25). Thus, our construct reports pH over the range required for SGs. Further calibration experiments found no dependence of the apparent pK_a of the probe on the luminal Ca^{2+} concentration; it was the same at 10 μM, 200 μM, and 2 mM (Fig. S1*D*). Comparing normalized fluorescence titrations on batches of PC12 cells expressing either D1-ER or D1-SG shows that these two probes traffic to cellular compartments of differing pH (Fig. 2*C*). The ER probe reports a pH of 6.9, whereas the granular probe reports a pH of 5.8. Because the pH is much lower in granules than in the ER (2), and because some manipulations might change the pH of SGs, from this point on, the Ca^{2+} values we report for SGs were obtained from FRETr values corrected point-by-point using the pH-dependent empirical calibration formulae described in *Materials and Methods*. We also give the ER pH values reported during the experiments, but it should be remembered that changes of pH values above 6.9 will not be recorded reliably using a probe with a pK_a of 5.8.

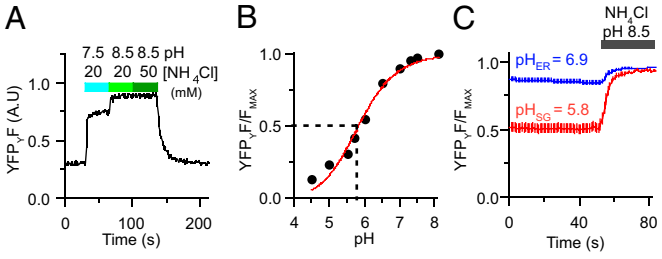

Fig. 2. Measuring granular pH from YFP fluorescence. (*A*) Brightness changes of YFP_Y in a cell transiently expressing D1-SG. Normal bath saline is changed to 20 mM NH_4Cl first at pH 7.5 and then at pH 8.5, and finally to 50 mM NH_4Cl at pH 8.5, progressively dequenching the YFP fluorophore (YFP_YF). A.U., arbitrary units. (*B*) In-cell titration of YFP_Y intensity as a function of pH. The fitted line is a Henderson–Hasselbalch curve with an apparent pK_a for citrine of 5.8. (*C*) Averaged YFP_Y fluorescence from PC12 cells expressing either ER localized D1-ER (blue trace) or SG localized D1-SG (red trace) normalized to the maximum fluorescence obtained with alkaline NH_4Cl treatment (20 mM, pH 8.5). Reported pH_{ER} = 6.9, pH_{SG} = 5.8 (n = 10 for ER, n = 15 for SG).

Comparing ER and SG Calcium. The two cameleon probes reported high but differing free-Ca^{2+} levels in their respective compartments. On average, free Ca^{2+} in the ER was higher than in the SG under basal conditions (285 ± 12 μM ER vs. 69 ± 15 μM SG). To validate the localization of the two probes functionally, we applied 50 μM tert-butyl-hydroquinone (BHQ) to inhibit the sarcoplasmic/endoplasmic reticulum Ca^{2+} ATPase (SERCA) or depolarized the PC12 cells with KCl. The SERCA pump opposes a continuous ER Ca^{2+} leak (24, 26). As shown in Fig. 3*A*, after application of BHQ, ER Ca^{2+} starts to run down as anticipated. With the same treatment, SG Ca^{2+} also decreases but to a lesser extent (Fig. 3*B*). The SG pH is not affected. The Ca^{2+} loss from the ER does not depend on extracellular Ca^{2+}; however, unexpectedly, the decline of SG Ca^{2+} with BHQ is much reduced without extracellular Ca^{2+}. We also tried another inhibitor of SERCA pumps, cyclopiazonic acid (CPA), which gave the same results as BHQ (Fig. S4). The effects of SERCA inhibitors would be consistent with two alternative interpretations. First, similar to the ER, SGs may have an appreciable Ca^{2+} leak and Ca^{2+} ATPase pumps sensitive to BHQ and CPA maintaining their high resting SG Ca^{2+}. Alternately, SGs might not use BHQ- and CPA-sensitive active transport; instead, they may have a Ca^{2+} release mechanism that is turned on indirectly by the effects of SERCA-pump inhibitors on the ER (*Discussion*).

Depolarizing PC12 cells with 100-s applications of KCl produces sustained Ca^{2+} elevations of several micromolars in the cytoplasm (27). Such KCl treatments did not change ER Ca^{2+} (Fig. 3*C*) or SG pH (Fig. 3*D*) but did cause the SG Ca^{2+} to increase gradually by 75% while the cytoplasmic Ca^{2+} was high (Fig. 3*D*). This slow increase in SG Ca^{2+} following KCl stimulation was reduced by 80% when BHQ was coapplied with KCl to cells also expressing a dominant-negative Orai1(E106A). These results show that SGs are capable of dynamic Ca^{2+} import, perhaps participating in the buffering of calcium during cytoplasmic elevations or depolarization. Also, because the total YFP_Y signal (used to determine SG pH) remains steady, we deduce that very few YFP-containing SGs are exocytosed during the KCl treatment.

ER and SG free Ca^{2+} was reversibly decreased by application of alkaline NH_4Cl. For the cytoplasm and ER, the NH_4Cl solution might raise the pH by ~1 pH unit (e.g., Fig. 2*C*) because their baseline pH is already near neutral. In response to the alkaline solution, the reported ER free Ca^{2+} drops suddenly by ~65% on average (Fig. 3*E*). More extremely, the alkaline NH_4Cl

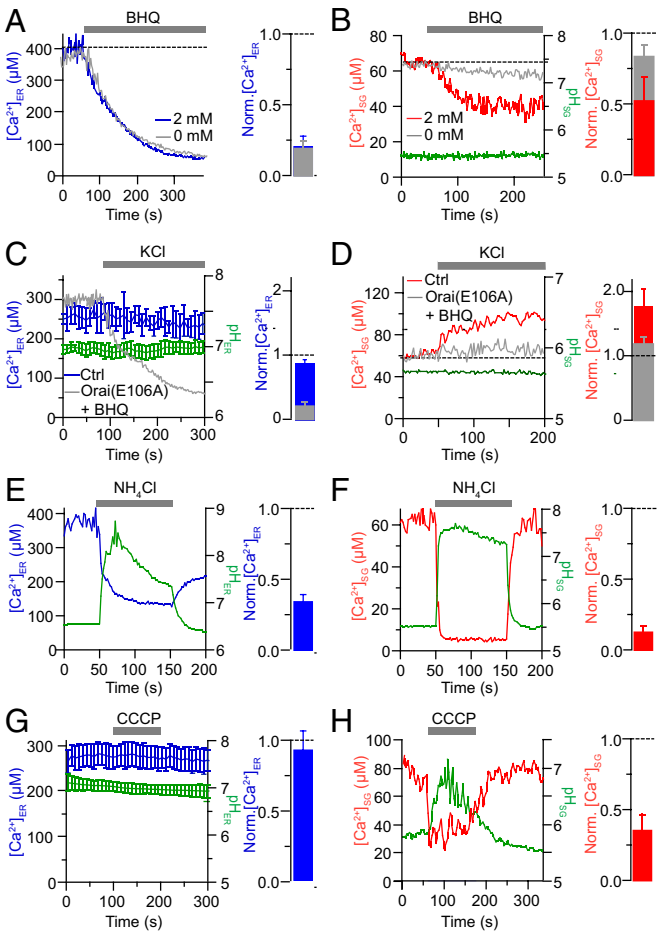

Fig. 3. ER and SG probes report independent pools of calcium. (*A*) Representative $[Ca^{2+}]_{ER}$ recording from a cell expressing D1-ER. BHQ (50 μM) is applied to inhibit the SERCA. The histogram displays summary data from this protocol (n = 8). (*B*) Representative $[Ca^{2+}]_{SG}$ and pH_{SG} records in a cell expressing D1-SG and treated with BHQ in the presence of 2 mM (red line) or 0 mM (gray line) extracellular Ca^{2+}. The histogram displays summary data from this protocol (n = 5). (*C*) $[Ca^{2+}]_{ER}$ was unaffected by prolonged 70-mM KCl treatment. BHQ was coapplied with KCl in cells overexpressing Orai1 (E106A) (gray line). Summary histogram (blue) displays normalized ER calcium (n = 6). (*D*) $[Ca^{2+}]_{SG}$ (red line) increased in response to KCl without any significant change in SG pH (green line). This response was reduced when BHQ was coapplied with the KCl (gray line) to cells overexpressing Orai1 (E106A). The summary histogram (red) displays normalized SG calcium (n = 7). (*E*) Average $[Ca^{2+}]_{ER}$ (blue) and pH_{ER} (green) responses during addition of 20 mM NH_4Cl at pH 8.5. The histogram displays summary data from this protocol (n = 10). (*F*) $[Ca^{2+}]_{SG}$ (red) and pH_{SG} (green) in a cell expressing D1-SG and treated with 20 mM NH_4Cl at pH 8.0. The histogram displays summary data from this protocol (n = 7). (*G*) Average $[Ca^{2+}]_{ER}$ (blue) and pH_{ER} (green) responses during addition of 2 μM CCCP. The histogram displays summary data from this protocol (n = 5). (*H*) $[Ca^{2+}]_{SG}$ (red) and pH_{SG} (green) in a cell expressing D1-SG and treated with 2 μM CCCP. The histogram displays summary data from this protocol (n = 5). Norm., normalized.

solution increases the measured pH in SGs by ~2 or more pH units (Fig. 2*C*) and the reported SG Ca^{2+} drops immediately by >90%, again quite reversibly (Fig. 3*F*). Could these changes represent an artifactual direct effect of NH_4Cl on our luminal probes? As a control, we collapsed organellar pH gradients with the proton ionophore, CCCP. The ER free Ca^{2+} and ER pH remained unchanged (Fig. 3*G*), whereas the SG pH quickly rose to values approaching cytoplasmic pH (~pH 7.0) as expected and SG free Ca^{2+} quickly fell by ~65% (Fig. 3*H*). The recovery of SG pH and Ca^{2+} following washout of CCCP was slower than for NH_4Cl. Thus, changes of ER and SG free Ca^{2+} seem to track and be due to changes of luminal pH, and they are largest for the more extreme pH changes of SGs. We reason that the abrupt and reversible changes of SG and ER free Ca^{2+} on alkalinization are due to a strong pH dependence of intraluminal Ca^{2+} buffer molecules (*Discussion*).

Slow Stimulated Release of Calcium from SGs. The key unresolved question concerning Ca^{2+} and pH in SGs is whether they change in physiologically interesting ways in response to signals. When we sought the answer to that question, we discovered a unique mode of Ca^{2+} release from SGs in response to receptor stimulation by ATP. Application of ATP stimulates plasma membrane P2Y purinergic receptors (28), initiates IP_3 production, and initiates a large Ca^{2+} release from intracellular Ca^{2+} stores. Let us begin by distinguishing rapid and slower components of the cytoplasmic Ca^{2+} rise observed using Fura-4F (Invitrogen) (Fig. 4*A*). The long Ca^{2+} rise in control Ca^{2+}-containing medium is much shortened when ATP is applied in nominally Ca^{2+}-free extracellular medium (Fig. 4*B*). Thus, the initial transient rise is due to rapid Ca^{2+} release from the ER and the smaller delayed component, requiring extracellular Ca^{2+}, would represent SOCE through plasma membrane channels. An approximate time course of SOCE is given by subtracting one record from the other (Fig. 4*B*). This delayed entry peaks around 25 s after ATP application. We then used our ER and SG probes to compare the Ca^{2+} responses of these organelles during the application of ATP. Interestingly, each responded, although differently; however, eventually, after 200 s of ATP treatment, Ca^{2+} had fallen significantly in both compartments (average Ca^{2+} before and after ATP was 278 ± 27 μM and 166 ± 31 μM for the ER and 67 ± 21 μM and 15 ± 9 μM for SGs).

Now, consider the time course of these changes. As anticipated, ATP initiated a quick transient loss of Ca^{2+} from the ER (Fig. 5*A*) that is coincident with the quick transient rise in the cytoplasm, presumably using IP_3 receptor channels. Then, in a quick rebound, Ca^{2+} was briskly taken back up again by the ER. However, within tens of seconds in the continued presence of ATP, ER Ca^{2+} began a secondary slow decline. In contrast, in response to the same stimulus, SG Ca^{2+} showed no changes during the initial phases of release and reuptake by the ER but then, only later, began a delayed slow monotonic decrease (Fig. 5*A*) unaccompanied by any SG pH changes. This loss of SG Ca^{2+} coincided temporally with the development of SOCE (Fig. 4*C*). To determine whether SOCE had some relation to the Ca^{2+} dynamics of ER and SG stores, we repeated the experiments using a Ca^{2+}-free medium. There were striking changes in both ER and SG signals. The ER Ca^{2+} no longer showed any rapid rebound; rather, the sharp initial release of Ca^{2+} was followed by continued slow net release (Fig. 5*B*). This result implies that the influx of extracellular Ca^{2+} by SOCE underlies the early recovery of ER Ca^{2+} during ATP application, a classic postulate (17). On the other hand, quite unexpectedly, the Ca^{2+}-free medium simply eliminated all changes in the SG Ca^{2+} in response to ATP. Again, the SG pH remained steady. Thus, paradoxically, the ATP-induced release of Ca^{2+} from SGs appears to be linked to SOCE.

Release of Ca^{2+} from SGs Requires Functional Orai Channels. We next tested the relation to SOCE by depressing or augmenting the formation of conducting Orai1 store-operated channels. First, we overexpressed the nonconducting dominant-negative mutant Orai1(E106A), where a conserved glutamate in the pore region is replaced by an alanine (20). Overexpression of the E106A mutant had the same effects on the ER and SG Ca^{2+} responses to ATP as Ca^{2+}-free medium. The ER Ca^{2+} no longer rebounded quickly following its initial fast release, and the SG Ca^{2+} remained high and steady (Fig. 5*C*). As a second test, we applied BTP2, an inhibitor of several ion channels, including SOCE (29). Again, BTP2 blocked the rapid rebound of ER Ca^{2+} during ATP ap-

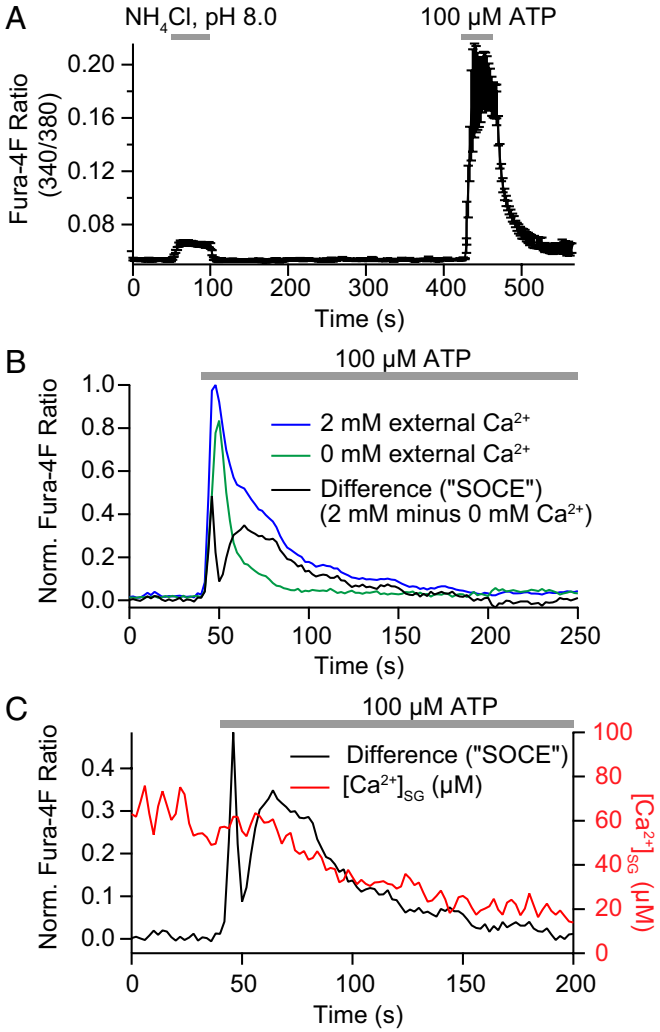

Fig. 4. Cytoplasmic Ca^{2+} transients during application of alkaline NH_4Cl or ATP. (*A*) Uncalibrated Fura-4F fluorescence ratio during a 50-s exposure to 20 mM NH_4Cl (pH 8.0) and a 40-s exposure to 100 μM ATP (average of $n = 6$). Cells had been loaded with Fura4F-AM. Exposure to NH_4Cl led to only a small increase in cytoplasmic calcium, whereas activation of endogenous purinergic receptors with ATP produced a much larger increase. (*B*) Normalized Fura-4F fluorescence ratio during a 200-s exposure to 100 μM ATP in a bath medium containing 2 mM Ca^{2+} (blue) or no added Ca^{2+} (green). The initial Ca^{2+} elevation is due to IP_3-mediated Ca^{2+} release from the ER. The much longer response with Ca^{2+}-containing medium is indicative of SOCE that follows once the ER free Ca^{2+} is significantly depleted. The SOCE component was estimated by subtracting the calcium response to ATP in no external Ca^{2+} from the response in 2 mM external Ca^{2+} (average of $n = 6$). (*C*) Comparison of the time course of SOCE (from *B*) with the time course of SG Ca^{2+}. The slow release of calcium from SGs occurs during SOCE. Norm., normalized.

plication and abolished the release of Ca^{2+} from SGs (Fig. 5*D*). With Orai1(E106A) and BTP2, the SG pH was constant during ATP application (Fig. 5 *C* and *D*). These three independent experiments, (*i*) Ca^{2+}-free medium, (*ii*) dominant-negative Orai1 (E106A), and (*iii*) an antagonist that can block SOCE collectively, suggest that Ca^{2+} entry through Orai1 channels is needed both for the early rebound of ER Ca^{2+} and for release of SG Ca^{2+}. To test this hypothesis further, we overexpressed the CRAC activation domain (CAD) of STIM1 (30). The CAD is a highly conserved 107-aa region of STIM1 that binds directly to Orai1 to open CRAC channels (30). Overexpression of the CAD resulted in a decrease of resting SG Ca^{2+} by ~75% (Fig. 5 *E* and *F*) and completely abolished the ATP-mediated release of Ca^{2+} from SGs (Fig. 5*E*). The resting concentration of SG Ca^{2+} with CAD overexpression is nearly identical to the depleted SG Ca^{2+} concentration following ATP application. The CAD construct caused no significant change in ER free calcium (Fig. 5*F*). Overexpression of a dominant-negative CAD construct (CAD-A376K) (31) that lacks the ability to bind or activate Orai1 induced no significant changes in ER or SG free Ca^{2+} (Fig. 5*F*). Collectively, we have three lines of evidence that functioning Orai channels are required for receptor-activated release of Ca^{2+} from SGs, and we show that the Orai-stimulating CAD suffices to deplete Ca^{2+} from SGs. Hence, we suggest a unique hypothesis for SG Ca^{2+} release (Fig. 5*G*) postulating Orai channels on SG membranes that can be opened by activated STIM1 in the ER membrane (*Discussion*).

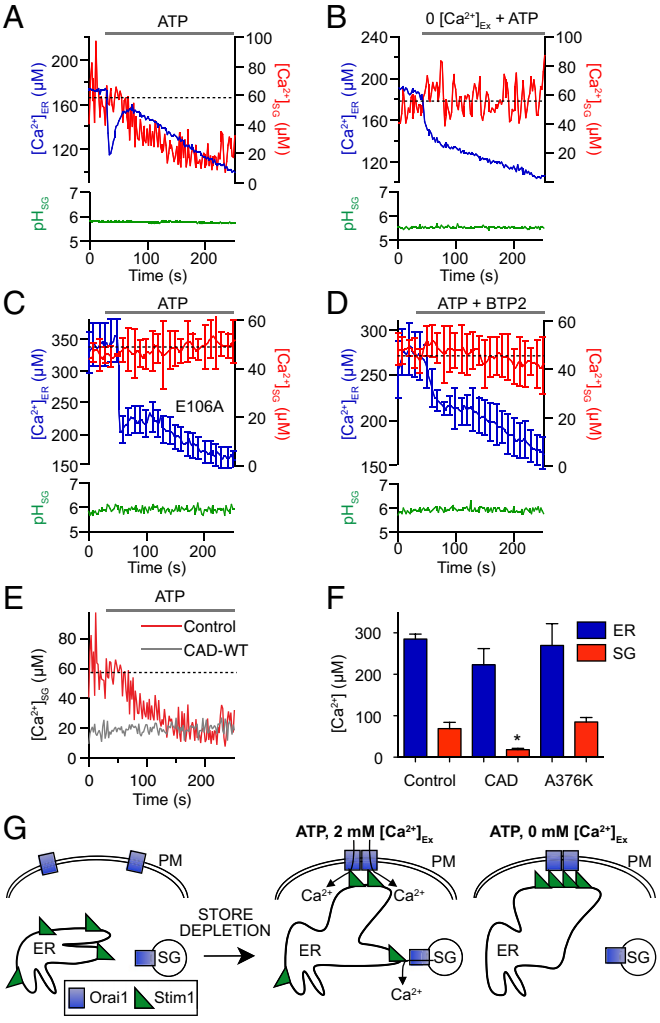

Fig. 5. Decline in $[Ca^{2+}]_{SG}$ following purinergic receptor activation suggests a store-operated release. Comparisons between different cells transfected with D1-ER or D1-SG. (*A*) $[Ca^{2+}]_{ER}$ (blue trace), $[Ca^{2+}]_{SG}$ (red trace), and pH_{SG} (green trace) during prolonged application of ATP (100 μM). (*B*) Like *A*, but with Ca^{2+}-free external medium. (*C*) Averaged responses of $[Ca^{2+}]_{ER}$, $[Ca^{2+}]_{SG}$, and pH_{SG} to ATP from cells overexpressing the dominant-negative Orai1 mutant Orai1(E106A). (*D*) Addition of ATP together with BTP2, a blocker of SOCE. (*E*) $[Ca^{2+}]_{SG}$ during prolonged application of ATP (100 μM), with (gray line) or without (red line; same data as in *A*) CAD-WT overexpression. (*F*) Summary of resting $[Ca^{2+}]_{ER}$ (blue bars) and $[Ca^{2+}]_{SG}$ (red bars) in cells expressing D1-ER or D1-SG either alone, with CAD-WT ($n = 6$), or with CAD-A376K ($n = 5$). (*G*) Model proposing $[Ca^{2+}]_{SG}$ release via Orai channels on SGs and regulation of Stim-Orai coupling by Ca^{2+} entry. Ex, extracellular; PM, plasma membrane.

Orai Channels Are Localized to SGs. We tested whether SGs express Orai1 channels by confocal colocalization analysis on cells overexpressing Orai1-GFP and tPA-mCherry. Three to five days after transfection, tPA-mCherry, serving as our marker for SGs, assumed a granular distribution (Fig. 6 *A–C*) similar to D1-SG and CgB staining in Fig. 1*C*, whereas Orai1-GFP was distributed both in the plasma membrane and in cytoplasmic, granular-like structures. Colocalization analysis was performed on cytoplasmic areas, with pixels close to the plasma membrane masked to avoid any coincidental colocalization between Orai-GFP and tPA-mCherry, both of which have the plasma membrane as their final destination. Our granular object analysis on such images revealed significant colocalization (33% ± 0.12) between tPA-mCherry– and Orai1-GFP–positive cytoplasmic structures (Fig. 6*D*). In the now standard description of SOCE, Orai1 channels of the plasma membrane are activated through an association with ER STIM1 following depletion of ER Ca^{2+} (reviewed in ref. 18) (Fig. 5*G*). To investigate whether SGs also possess STIM1, we overexpressed tPA-mCherry with STIM1-GFP. The tPA-mCherry again assumed a granular distribution, whereas STIM1-GFP assumed its predicted ramifying pattern across the ER network at rest (Fig. 6*B*). Merging the D1-SG and STIM1 wavelength channels (Fig. 6*B*) revealed complementary patterns rather than overlap. Accordingly, granular object analysis based on tPA-mCherry granular objects found negligible colocalization (>1%) between tPA-mCherry and STIM1-GFP (Fig. 6*D*). Whereas the granular object analysis is ideally suited for punctate structures that have defined centers, it may be less appropriate for STIM1 aggregates that assume larger plaque-like distributions (Fig. 6*B*). Therefore, we also used Pearson's correlation analysis, confirming little colocalization between tPA-mCherry and STIM1-GFP at rest (Fig. 6*E*, control). The above quantitative analyses can be illustrated qualitatively by comparing line scans from individual red and green images. Line scan analysis shows fluorescence intensities of Orai1 and tPA-mCherry rising and falling in parallel (Fig. 6*A*, regions 1–3). In contrast, fluorescence intensities of tPA-mCherry rise where there are reductions in STIM1 intensity (Fig. 6*B*, areas 1–3). Thus, there is a high percentage of colocalization between SGs and Orai1 but not between SGs and STIM1 at rest. Next, we wanted to determine whether ATP caused SGs and STIM1 to associate (Fig. 5*G*). We found that colocalization between SGs (tPA-mCherry) and STIM1-GFP increased significantly (control: $r = 0.13 \pm 0.01$; ATP: $r = 0.42 \pm 0.03$) during ATP treatment (Fig. 6 *C* and *E*). Line scan analysis revealed that tPA-mCherry intensity rises together with STIM1 intensity (Fig. 6*C*, areas 1–3). These results are consistent with the concept of Orai1 channels on SGs that join up with activating STIM1 in the ER during

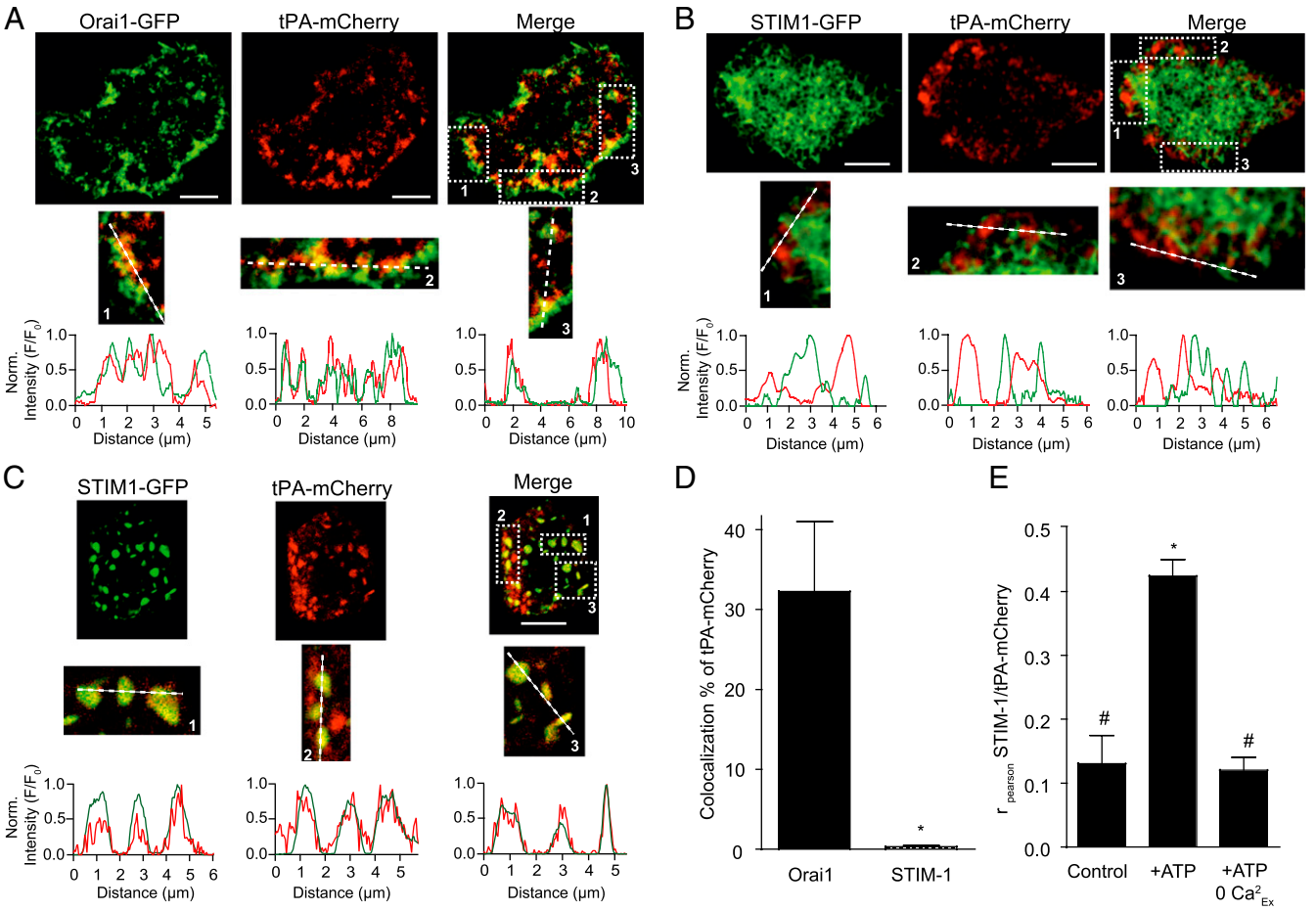

Fig. 6. SGs colocalize with Orai1 and recruit STIM1. (*A*) Representative confocal images from PC12 cells expressing Orai1-eGFP (green, *Left*), tPA-mCherry (red, *Center*), and merge (*Right*). Line scans were taken from areas (dashed squares 1, 2, and 3 in merge column) exhibiting high colocalization of both plasmids and show profiles of fluorescence intensity against line distance. (*B*) Representative confocal images from PC12 cells expressing STIM1-eGFP (green, *Left*), tPA-mCherry (red, *Center*), and merge (*Right*). Line scans were taken from marked areas (1–3). (*C*) Representative confocal images from PC12 cells expressing STIM1-eGFP (green, *Left*), tPA-mCherry (red, *Center*), and merge (*Right*) taken in the presence of 100 μM ATP. Line scans are from marked areas (1–3). (*D*) Summary of colocalization between tPA-mCherry and Orai1 and STIM1 using granular object based analysis. (*E*) Summary of colocalization between tPA-mCherry and STIM in control, ATP, and ATP-Ca^{2+}-free conditions using Pearson's correlation analysis. (Scale bars: 10 μm.)

purinergic receptor activation. As anticipated, the increase in colocalization between SG and STIM1 did not occur with ATP application in Ca^{2+}-free medium ($r = 0.12 \pm 0.02$; Fig. 6*E*).

Discussion

We developed a unique optical probe that measures Ca^{2+} and pH in SGs of living cells. It has appropriate Ca^{2+} and pH sensitivity and localizes primarily to SGs. As expected, it reports a high resting intragranular free Ca^{2+} and a low pH. We discovered (*i*) active (uphill) transport of Ca^{2+} into SGs when cytoplasmic Ca^{2+} is elevated, (*ii*) a slow release of Ca^{2+} from SGs that occurs upon treatment with the SERCA-pump inhibitors BHQ and CPA, and (*iii*) a slow receptor-stimulated release of Ca^{2+} that occurs secondary to ER store depletion and depends on functional Orai channels. We find that SGs have Orai channels. We propose that Orai on the granules can be opened secondarily after STIM has sensed Ca^{2+} depletion in the ER and has opened Orai channels of the plasma membrane (Fig. 5*G*). The details of this hypothesis are amplified toward the end of this section. In addition, using the established D1-ER probe, we observed an expected early Ca^{2+} release from ER after purinergic receptor stimulation, followed by a fully SOCE-dependent rapid rebound refilling even in the presence of agonist. Although some kind of SOCE-dependent refilling has long been proposed (17), the kinetics have not previously been seen so directly and with such clarity. No physiological stimulus was found to affect SG pH.

D1-SG Probe Localization. How well is the newly developed probe localized to SGs? A key feature of genetically encoded probes is their ability to be targeted. However, secreted proteins are synthesized in the ER and trafficked via the Golgi before being packaged in SGs, and at a later time, they may be partially exocytosed and recaptured into an endosomal or recycling pool. Thus, the localization of our probe should depend on how many hours one waits after transfection. The experiments of this study were done after 48–72 h, when the disposition of D1-SG appeared granular. Colocalization of various immune markers with our probe was analyzed by pixel cross-correlation and by distance analysis of granular objects, as well as by qualitative line scans. Each criterion showed a clear and significant majority of D1-SG fluorescence in SGs. Not all granules staining with CgB were detectably labeled with D1-SG. It is quite possible that they represent cohorts of SGs that originated before probe expression began or after it was over. There was poor colocalization between D1-SG and the ER marker (GRP78), the organelle where the probe is initially synthesized, and our functional observations all argue against significant contamination from ER signals. For example, D1-SG and D1-ER probes reported striking differences in ambient pH and Ca^{2+} and different Ca^{2+} responses to alkalinization, activation of purinergic receptors, disruption of SOCE, and depolarization with KCl. Organelle markers for early endosomes and for lysosomes showed minor overlap above the $P = 0.05$ level but several fold lower overlap than for the CgB marker of SGs. Weak partial localization with EAA1 occurred in regions near the plasma membrane and could be due to exocytosis of SGs followed by endocytosis into endosomes. The probe was not in large endosomes distal from the plasma membrane. Weak partial localization with LAMP-2 could be due to eventual recycling of older probe molecules. Methodological cautions on using the D1-SG probe are given in *SI Materials and Methods*.

Calcium Uptake and Buffering by SGs. To be considered a calcium store, an organelle should have an appropriate apparatus for calcium uptake, storage, and release. Acidic granules, including SGs, sequester calcium and buffer it well. They are thought to do so through exchangers, pumps, and matrix molecules (11, 15, 16). Our value for SG resting Ca^{2+} (~70 μM) fits nicely with earlier estimates using a low-affinity aequorin reporter or small chemical indicators as summarized in Table S1. Also, we found unique evidence for active transport of Ca^{2+} into SGs. When the cytoplasmic Ca^{2+} was elevated to micromolar levels by prolonged depolarization, the SG Ca^{2+} increased markedly over tens of seconds. In an earlier paper (32), we had proposed that Ca^{2+} is taken up into acidic stores during 30-s KCl depolarizations of these cells. Transient, dynamic overfilling of these stores was postulated to explain a cytoplasmic Ca^{2+} "hump" or plateau that delayed full Ca^{2+} clearance from the cytoplasm after the depolarization as the acidic store gradually lost its extra load. Our observations here seem to verify that concept. In addition, we found that this slow uptake of Ca^{2+} into SGs was reduced by 80% following the simultaneous application of BHQ with KCl. Typically, BHQ would also allow ER Ca^{2+} to be depleted, activating STIM and SOCE. To avoid the possible side effects of STIM acting on SGs, the KCl-BHQ experiment was done in cells overexpressing a dominant-negative Orai(E106A) channel (Fig. 5*D*). The Ca^{2+} uptake into SGs was reduced in the presence of BHQ, as would be consistent with the concept that SGs use SERCA pumps.

Consider next the decrease in SG Ca^{2+} that occurs when SERCA pumps are inhibited. We see two possibly coexisting explanations: (*i*) There may be SERCA pumps on SGs, such that uptake of Ca^{2+} is stopped directly by BHQ and CPA, and (*ii*) SERCA inhibitors may promote Ca^{2+} release indirectly by ER store depletion, activating STIM and opening SG Orai channels. We find evidence for both possibilities. Consider the kinetics. Following ATP treatment, which does deplete ER Ca^{2+}, the slow loss of SG Ca^{2+} takes some time to begin (20–50 s) and SG Ca^{2+} ultimately decreases by 75–80%. Because SERCA-pump inhibitors are a conventional stimulus to deplete Ca^{2+} stores and induce SOCE, it seems inevitable that SERCA inhibitors will also activate the Orai-dependent indirect route of SG Ca^{2+} release (the second explanation), but only after a delay. Because the decline of SG Ca^{2+} with BHQ begins as soon as 10 s, we suggest that at least an early component of the loss is due to direct inhibition of SERCA pumps resident on SGs (first explanation). To explore the relative contributions of SERCA vs. Orai-STIM in mediating SG Ca^{2+} release during BHQ treatment further, we removed extracellular Ca^{2+}, a condition we know eliminates the Orai-STIM–mediated Ca^{2+} release from granules (Fig. 5*B*). In the absence of extracellular Ca^{2+}, BHQ caused a much smaller release of Ca^{2+} from SGs. Taken together, these experiments would be consistent with dual actions of SERCA inhibitors: early and direct on the SG pumps and later and indirect by opening SG Orai channels.

Because the total Ca^{2+} in SGs is usually put in the range 30–40 mM (8, 9), the effective Ca^2 binding ratio of granular Ca^{2+} buffering molecules would be as high as 1:500 at granular pH and much higher at the elevated pH induced by the alkaline medium. Some Ca^{2+} chelation within acidic vesicles may occur through abundant phosphate and sulfate groups, which are strong acids that can form complexes even at low pH. Also, in general, polyanionic matrices (33), including polyphosphates and proteins like chromogranin (34), melanin (35), and mucin (13), have been implicated in acidic granular calcium buffering.

Effect of Alkaline Ammonia. Our probes report an abrupt and large decrease of SG free Ca^{2+} during addition of alkaline NH_4Cl solutions and a parallel but smaller decrease in the ER. What is the mechanism? Because the response in the two compartments is similar, we assume that the same explanation applies to both. We consider two alternative hypotheses. The first is the Ca^{2+}-release hypothesis as follows. Without a pH gradient, SGs and the ER lose much of their total Ca^{2+} very rapidly, and when the pH gradient is restored, proton-driven transport restores the Ca^{2+} very quickly. In this hypothesis, a major quantity of released Ca^{2+} should appear in the cytoplasm immediately during alkalinization and be quickly removed on removal of NH_4Cl. Also, there would need to be a proton-driven Ca^{2+} pump in both the ER and SG membranes. This release hypothesis is contradicted by several observations. First, we did not find a large, immediate cytoplasmic

Ca^{2+} elevation. Although D1-SG and D1-ER report a very much larger decrease of Ca^{2+} within SGs and the ER with alkalinization than during ATP application, the application of NH_4Cl initiates only a very modest ~20-nM increment of the cytoplasmic free Ca^{2+} (Fig. 4*A*). This tiny change can be compared with that evoked when receptor signaling evokes bona fide Ca^{2+} release from intracellular stores. The cytoplasmic transient evoked by ATP is almost 10-fold larger than that evoked by alkalinization. Second, the reversible changes with pH seem quicker than a release and reuptake mechanism might be expected to be. Compare, for example, the slowness of the Ca^{2+} release in response to SERCA inhibitors in Fig. 3 *A* and *B*. Finally, the neutral luminal pH and the lack of change of ER free Ca^{2+} in response to CCCP treatment suggest that ER membranes are not using proton-driven Ca^{2+} pumps. We reject the release hypothesis.

The second hypothesis is the Ca^{2+}-buffer hypothesis as follows. The powerful Ca^{2+} buffers in granules and the ER bind Ca^{2+} much better after they are deprotonated by the alkaline treatment. In this hypothesis, there is no rapid Ca^{2+} efflux across the compartment membranes, just a nearly instantaneous augmentation of the Ca^{2+} binding ratio of the luminal buffer at high pH. Favoring this hypothesis is the speed of the changes in free Ca^{2+} and the contradictions of the release hypothesis. We note that after short fluid-phase loading of conventional indicator dyes into macrophages, Christensen et al. (36) reported precipitous endolysosomal Ca^{2+} drops and a minor cytoplasmic Ca^{2+} increase (40 nM) exactly like ours in response to NH_4Cl solutions. When endolysosomal pH rose from 4 to 7, the organellar Ca^{2+} dropped reversibly and immediately by 100-fold in macrophages. Although their interpretation was that neutralized acidic compartments might release Ca^{2+}, we suggest that the effect of removing protons on buffers be considered there too.

Calcium Release from SGs Is Not via IP_3 Receptors. We come finally to the delayed slow decline of Ca^{2+} from SGs during exposure to ATP. This we regard as a genuine slow Ca^{2+} release from SGs. The possibility of stimulated Ca^{2+} release from SGs has remained controversial (Table S1). IP_3-mediated calcium release or oscillations and calcium-induced calcium release (CICR) from SGs have been favored by some authors (10, 12–14, 34, 37–39) and contested by others (11, 40). Differences in their results may reflect different species, preparations, and cell types. Studies on isolated granule preparations may have included contaminating ER fragments, and in intact cell studies with an ATP stimulus, the response may not have been due to the actual direct action of IP_3. A significant source of difficulty has been in monitoring SG calcium conveniently, a problem that wider use of our D1-SG probe might solve now.

We start with arguments that the release we see is neither IP_3 receptor-mediated release nor CICR. If it were due to opening of conventional IP_3 receptor Ca^{2+} release channels, it should be synchronous with the generation of IP_3 and parallel the early IP_3-dependent release from the ER. However, the release from SGs is delayed (starting after 25–50 s) and slow. That from the ER begins almost at once, like the expected production of IP_3, and clearly precedes the release from SGs. Furthermore, the release from SGs is completely stopped by four maneuvers that stop or activate SOCE: Ca^{2+}-free medium, dominant-negative Orai1, blocker BTP2, and CADs. None of these interventions alters the IP_3-induced initial Ca^{2+} release from the ER. These differences are evident both from our intraluminal Ca^{2+} measurements on the two organelles and from the cytoplasmic Ca^{2+} measurements. Thus, using our newly developed tool in PC12 cells has provided no support for the oft-presented conclusions of Yoo (34) that the majority of IP_3 receptors in secretory cells are on SGs and that IP_3 releases more calcium from SGs than from the ER and nucleus. The same experiments argue against a release mechanism based on CICR. The cytoplasmic Ca^{2+} transient during ATP is fast and sharp and becomes briefer but not lower in Ca^{2+}-free medium. Nevertheless, the SG Ca^{2+} release waits for the falling phase of the cytoplasmic transient, persists after Ca^{2+} has fallen to low levels, and is absent in Orai1-disrupting conditions. These are not properties of CICR. Furthermore, the cytoplasmic Ca^{2+} elevation induced by KCl solution fails to evoke any loss of Ca^{2+} from SGs. In fact, the SGs gain Ca^{2+}.

Ca^{2+} Release Uses Orai Channels. How is SG Ca^{2+} released during ATP stimulation? Our observations seem not only to rule out second-messenger actions, such as direct actions of IP_3 or phosphorylation of SERCA on SGs by PKC, but to implicate Orai channels and SOCE: ATP-induced release from SGs stops when Orai1 function is blocked, and it is mimicked and occluded by the CAD. The release mechanism in SGs seems to require prior ER store depletion and SOCE by plasma membrane Orai channels. This would explain the delayed time course of Ca^{2+} release from SGs.

What is the release channel that opens on the SGs, and how is it regulated? The summary cartoons of Fig. 5*G* present our working hypothesis that the membranes of SGs use Orai1 as their Ca^{2+} release channel. A database search for sequence motifs in Orai that might target it to SGs was negative. Nevertheless, by confocal colocalization, we found evidence that Orai1 is present on SGs. Following the conventional activation of SOCE by STIM at the plasma membrane, the postulated sequence of events would be as follows. Some active STIM1 molecules are released from their tight complex with plasma membrane Orai as the local Ca^{2+} rises there (22, 23). They become available for interaction with low-density Orai1 on SGs. We believe that the increase in colocalization between tPA-mCherry and STIM1 during ATP treatment represents this interaction. Now, the SG population of Orai channels becomes activated, initiating a delayed loss of Ca^{2+} from SGs. Given that free Ca^{2+} in SGs is only 1/20th that in the external medium, the flux per SG Orai channel may be only 1/20th that at the plasma membrane Orai channels. This Ca^{2+}, released locally where SG Orai has become coupled with ER STIM, could be rapidly pumped back into the closely apposed ER, providing another mechanism for refilling of the ER. SG Ca^{2+} is probably released too gradually to have much impact on global cytoplasmic Ca^{2+}; however, it might have local actions. In Ca^{2+}-free solutions or with inhibited Orai channels, SOCE Ca^{2+} entry from outside is absent and the aggregation of STIM and Orai at the plasma membrane remains tight and traps all the STIM, such that none is available for the secondary complex with SGs. With overexpression of the CAD, SG Ca^{2+} is significantly lowered, presumably by chronic opening of Orai1 channels on SGs. It has been reported that STIM1 and STIM2 are present on acidic calcium stores as well as on the plasma membrane and that selective depletion of acidic stores induces translocation and enhanced association of STIM1 on acidic stores with plasma membrane Orai1 (41). However, in our cells, we found very little resting colocalization of STIM1 with SGs by confocal microscopy.

What is the physiological role of Orai channels on SGs? This question remains to be elucidated. It is possible that they are most important as cargo to be deposited on the plasma membrane to participate in the canonical plasma membrane SOCE paradigm. If so, the changes we observe of luminal SG Ca^{2+} could be seen as due to chance proximity of SGs to activated STIM1 molecules. Even if it is mostly such an epiphenomenon, this could have important functional consequences. The released Ca^{2+} could contribute to local calcium elevations, aiding in regulating exocytosis and in refilling ER calcium stores. We saw no large decrease in YFP_Y fluorescence that might signal some mass exocytosis; however, as is typical of PC12 cells, it is very likely that there was exocytosis at the level of only a few vesicles (42).

The importance of understanding Orai signaling is clear. Some patients with SCID syndrome have defective SOCE due to a single missense mutation in Orai1 (43). Many other diseases and processes, such as tumor metastasis (44), vascular smooth

muscle proliferation (45), and triggering of apoptosis (46), depend on strict regulation of the Orai–STIM1 interaction. With the discovery that SGs, and perhaps other organelles, use Orai–STIM interactions for Ca^{2+} release, it seems likely that diseases or mutations that disrupt Orai or STIM signaling could alter calcium fluxes through Orai channels in more places than just the plasma membrane.

Materials and Methods

Cells and Transfection. The lineage and subculturing of the PC12 D19 cells are given by Duman et al. (27). Briefly, PC12 cells were maintained in DMEM (Invitrogen), supplemented with 5% (vol/vol) horse serum (Gemini Bioproducts), 10% FBS (vol/vol) (Gemini Bioproducts), 44 mM sodium bicarbonate, and 25 mM Hepes (pH 7.3) with NaOH. Cells were subcultured twice per week at a 1:6 dilution by trituration in culture medium. PC12 cells were transiently transfected with 3 μg of DNA using Lipofectamine 2000 (Invitrogen) according to the manufacturer's protocols and then subcultured onto poly-L-ornithine–coated cover glass (no. 0; Thomas Scientific) 24 h later. The granular probes did not assume a granular localization until 48 h posttransfection; therefore, all FRET photometry was performed 48 or 72 h posttransfection. All experiments and calibrations were performed at 35–37 °C.

Constructs. D1-ER (24) was from Roger Y. Tsien (University of California at San Diego, La Jolla, CA). Using standard molecular techniques, we created D1-SG by removing the C-terminal ER retention motif of D1-ER and replacing its N-terminal ER signal sequence with full-length rat tPA (provided by Wolfhard Almers, Vollum Institute, Portland, OR) (Fig. 1*A*). Other constructs were as follows: CAD and CAD-A376K (provided by Richard Lewis, Stanford University, Stanford, CA), rat tPA-mRFP (provided by Wolfhard Almers), human Myc-hOrai1-E106A (provided by Shenyuan Zhang, Texas A&M University, College Station, TX), human STIM1-EGFP, and human Orai1-EGFP.

Photometric Measurements. FRET and calcium measurements involved photometry, where photodiodes detected total light integrated over a detection region that included most of one cell image. Experiments were performed on the stage of an inverted epifluorescence microscope (47). For FRET, excitation light was provided using a Polychrome IV (TILL Photonics) and a three-color dichroic mirror reflecting at 440, 500, and 580 nm (89006bs; Chroma). Fluorescence emission was split between two photodiodes (TILL Photonics) by a DCLP505 dichroic mirror and sampled by Patchmaster (HEKA). The short-wavelength measurement channel (CFP) contained a D480/40 emission filter, and the long-wavelength channel (YFP) contained an ET535/30 filter (Chroma). For near-simultaneous sampling of CFP_C (440-nm excitation, 480-nm emission), raw YFP_C (440-nm excitation, 535-nm emission), and YFP_Y (500-nm excitation, 535-nm emission), the excitation wavelength was scanned in a ramp from 300 to 500 nm in 500 ms every 1 s and the photodiode voltages were averaged for each sweep during the time when excitation was between 420 and 450 nm and between 490 and 500 nm. After each measurement, an area of coverslip without cells was measured as background. After background subtraction, we corrected raw YFP_C for CFP emission collected in the long-wavelength channel by measuring cells expressing only CFP. The correction factor was 0.73*CFP_C. The corrected value is referred to as the YFP_C. As before (47), FRET was expressed as FRETr = YFP_C/CFP_C.

Calcium. Cytoplasmic free Ca^{2+} was measured by photometry using the low-affinity indicator Fura-4F (Invitrogen). For calcium measurements, cell-permeant Fura-4F-AM ester was diluted to 2 μM in Ringer's solution containing 0.2% pluronic F-127. Cells were loaded for 40 min and then incubated in regular Ringer's solution for a further 30 min to allow complete de-esterification of AM esters. Fura-4F fluorescence was measured by epifluorescence, stepping to 340-nm excitation for 100 ms and to 380-nm excitation for 20 ms every 2 s. After data acquisition, an area of the coverslip without cells was measured as background. Background fluorescence was then subtracted, and the ratio of emission with 340-nm excitation (F_{340}) to emission with 380-nm excitation (F_{380}) was calculated. Both the FRETr and Fura-4F ratio were calculated offline using a custom macro for IGOR Pro-6.0 (Wavemetrics).

Immunocytochemistry. Cells expressing D1-SG were fixed with 3.7% (vol/vol) formaldehyde for 10 min at room temperature 3 or 4 d after transfection. Cells were permeabilized with 0.3% Triton X-100 for 10 min and blocked with 5% BSA (vol/vol). Primary antibodies against the antigens listed in Fig. 1C were from Santa Cruz Biotechnology: SG, CgB (SC-1489); ER, GRP78 (SC-1050); Golgi apparatus, GM130 (SC-16271); trans-Golgi network, TGN38 (SC-27680); EE, EEA1 (SC-6414); lysosomes, LAMP-2 (SC-8100); and mitochondria, Mcl-1 (SC-819). Primary antibodies were detected using Alexa Fluor 568 rabbit anti-goat secondary antibodies (Invitrogen). Fixed cells were imaged on a Zeiss LSM 510 Meta confocal microscope using an argon ion laser to excite D1-SG and a helium neon laser to excite the secondary antibodies. Following acquisition, images were deconvolved using a deconvolution plug-in (DeconvolutionLab) available for ImageJ (National Institutes of Health).

Confocal Recordings. Confocal experiments on live cells were conducted at 37 °C in modified Ringer's solution using a Zeiss 710 laser scanning confocal microscope. STIM1-GFP and tPA-mCherry were excited with 488-nm and 561-nm laser lines, respectively. Scanned images were acquired using a 63× oil immersion lens, recorded using Zen software, and deconvolved (see above).

Method for Estimation of Colocalization of Granular Objects in Images. Our method to detect colocalization based on granular objects is closely derived from that of Zhang et al. (48). In brief, the two image channels to be compared are smoothed [improved à-trous wavelet (49)] and used to identify granular objects within the area of the cell. A weighted centroid calculation determines the center of each identified object. The subsequent analysis is completely based on the center-to-center distance of each object in one image channel to objects in the other channel. A criterion distance is determined separately for each image by means of a Monte Carlo calculation (1,000 randomly placed spots) for $P < 0.05$ occurring by chance. Puncta within this criterion distance are considered colocalized (e.g., puncta marked in yellow in Fig. S2 *C* and *D*). For each cell, the percentage of puncta colocalized of all the puncta is determined, and the results are expressed as mean and statistics of the colocalization percentage for all cells.

Calcium Calibrations. The fluorophore and sensor regions of D1-ER and D1-SG are identical. We performed Ca^{2+} calibrations on D1-ER and used that calibration for D1-SG. D1-ER was transfected transiently into PC12 cells. At 48 h posttransfection, cells were treated with 5 μM digitonin, 20 μM ionomycin, and 1 μM thapsigargin for 20 min in KCl-based solutions appropriately buffered at pH 7.4, 7.0, 6.5, 6.0, or 5.5 containing a free calcium concentration of 0 μM, 10 μM, 30 μM, 90 μM, 270 μM, or 5 mM. The FRETr was then recorded from at least 20 cells per condition at 37 °C as described above. Empirical calibration equations were developed as described below. The pH- and Ca^{2+}-buffered solutions were designed using Winmaxc.exe (Chris Patton, Stanford University, Stanford, CA). Solutions of pH 6.5 or greater were buffered with 20 mM Hepes, and those below pH 6.5 were buffered with 20 mM MES.

pH Calibrations. The pH calibrations were conducted on SG-targeted constructs. The pH is a single-wavelength measurement of citrine emission (535 nm) after direct citrine excitation (500 nm). Cells were transfected with D1-SG, and YFP_Y emission was measured 48 or 72 h after transfection. A standard curve was constructed by clamping pH in digitonin (5 μM)-permeabilized cells using strongly pH-buffered solutions and nigericin (10 μM) to equilibrate pH across the granular membrane (Fig. 2*B* and Fig. S1*D*). In addition, after every experiment, the unquenched fluorescence value of YFP_Y was calculated by deprotonating the citrine using a solution containing 20 mM ammonium chloride buffered to either pH 8.0 or pH 8.5. The pH was then calculated according to the standard curve from YFP_Y points collected throughout the experiment.

Empirical Curve Fitting of the Calibration Data. The D1-SG probe has a FRET response that depends on both the pH and Ca^{2+} concentration (Fig. 1*B*). For practical use, we developed an empirical formula to translate the FRET measurements into Ca^{2+}, given a known value of pH. First, the calibration points at each pH were fitted with the empirical equation

$$\mathrm{FRET}\left(\mathrm{Ca}^{2+}\right)_{\mathrm{pH}} = \mathrm{FRET}_{\mathrm{max,pH}} - \mathrm{Ampl}_{\mathrm{pH}} * \exp\left(-\mathrm{Ca}^{2+}/\mathrm{K}_{\mathrm{Ca,pH}}\right). \quad [1]$$

This yielded the empirical smooth curves in Fig. 1*B* and three coefficients ($FRET_{max,pH}$, $Ampl_{pH}$, and $K_{Ca,pH}$) at each of the five tested pH values. Next, the three coefficients were plotted as a function of pH (Fig. S1, symbols) and fitted with second-order polynomials (quadratic) (Fig. S1, smooth curve) of the form

$$\mathrm{Coeff} = \mathrm{k}_0 + \mathrm{k}_1 * \mathrm{pH} + \mathrm{k}_2 * \mathrm{pH}^2. \quad [2]$$

With these polynomial functions, it was possible to calculate the coefficients at any pH. The free Ca^{2+} for any FRET measurement could then be calculated as

$$Ca^{2+} = K_{Ca,pH} * \ln\left(Ampl_{pH}/\left[FRET_{max,pH} - FRET_{pH}\right]\right). \quad [3]$$

Because of the necessary differences in light sources, filters, and collection efficiency, these calibrations need to be measured and the equations fitted for each change in the measuring apparatus. A physically more elegant approach would be to fit calibration data like those in Fig. 1*B* with more complex binding curves rather than an empirical exponential and to proceed with the additional resulting coefficients in a similar manner. Further methodological considerations on the use of D1-SG are provided in *SI Materials and Methods*.

Pharmacological treatments. All pharmacological treatments of living cells were performed at 37 °C, and solutions were applied via local perfusion. Chemicals were dissolved or suspended in Hepes-buffered modified Ringer's solution [130 mM NaCl, 2.5 mM KCl, 2 mM $CaCl_2$, 1 mM $MgCl_2$, 10 mM Hepes, 10 mM glucose (pH 7.4)].

Analysis and statistics. Data were analyzed using IGOR Pro software and ImageJ. Mean ± SEM values were shown, and significance was assessed by the Student *t* test. Differences were considered significant when $P < 0.05$.

ACKNOWLEDGMENTS. We thank Drs. Michael Ailion, Wolfhard Almers, Barbara E. Ehrlich, Björn H. Falkenburger, Martin Kruse, Duk-Su Koh, Terry E. Machen, Alex J. Merz, and Erwin Neher for valuable discussions. We thank Lea Miller and Minh Huynh for technical assistance, Ken Mackie and Angela Boice for help with molecular biology, and Drs. Rose E. Dixon, Eric Senning, and Greg Martin for advice with microscopy. This work was supported by National Institutes of Health (NIH) Grants GM083913 and NS08174 (to B.H.), NIH Grants F32 DC068982 and K01 MH086119 (to J.G.D.), National Science Foundation of China Grants 30871225 and 81222020 and National Key Technology R&D Program SQ2011SF11B01041 (to L.C.), and NIH Grant RR025429 (to Sharona E. Gordon).

1. Macrez N, Mironneau J (2004) Local Ca^{2+} signals in cellular signalling. *Curr Mol Med* 4(3):263–275.
2. Wu MM, et al. (2001) Mechanisms of pH regulation in the regulated secretory pathway. *J Biol Chem* 276(35):33027–33035.
3. Dittie AS, Hajibagheri N, Tooze SA (1996) The AP-1 adaptor complex binds to immature secretory granules from PC12 cells, and is regulated by ADP-ribosylation factor. *J Cell Biol* 132(4):523–536.
4. Verdugo P (1990) Goblet cells secretion and mucogenesis. *Annu Rev Physiol* 52:157–176.
5. Holroyd P, Lang T, Wenzel D, De Camilli P, Jahn R (2002) Imaging direct, dynamin-dependent recapture of fusing secretory granules on plasma membrane lawns from PC12 cells. *Proc Natl Acad Sci USA* 99(26):16806–16811.
6. Perrais D, Kleppe IC, Taraska JW, Almers W (2004) Recapture after exocytosis causes differential retention of protein in granules of bovine chromaffin cells. *J Physiol* 560 (Pt 2):413–428.
7. Taraska JW, Perrais D, Ohara-Imaizumi M, Nagamatsu S, Almers W (2003) Secretory granules are recaptured largely intact after stimulated exocytosis in cultured endocrine cells. *Proc Natl Acad Sci USA* 100(4):2070–2075.
8. Hutton JC, Penn EJ, Peshavaria M (1983) Low-molecular-weight constituents of isolated insulin-secretory granules. Bivalent cations, adenine nucleotides and inorganic phosphate. *Biochem J* 210(2):297–305.
9. Winkler H, Westhead E (1980) The molecular organization of adrenal chromaffin granules. *Neuroscience* 5(11):1803–1823.
10. Gerasimenko OV, Gerasimenko JV, Petersen OH, Tepikin AV (1996) Short pulses of acetylcholine stimulation induce cytosolic Ca^{2+} signals that are excluded from the nuclear region in pancreatic acinar cells. *Pflugers Arch* 432(6):1055–1061.
11. Mitchell KJ, et al. (2001) Dense core secretory vesicles revealed as a dynamic $Ca^{(2+)}$ store in neuroendocrine cells with a vesicle-associated membrane protein aequorin chimaera. *J Cell Biol* 155(1):41–51.
12. Moreno A, et al. (2005) Calcium dynamics in catecholamine-containing secretory vesicles. *Cell Calcium* 37(6):555–564.
13. Nguyen T, Chin WC, Verdugo P (1998) Role of Ca^{2+}/K^{+} ion exchange in intracellular storage and release of Ca^{2+}. *Nature* 395(6705):908–912.
14. SantoDomingo J, et al. (2010) Ca^{2+} dynamics in the secretory vesicles of neurosecretory PC12 and INS1 cells. *Cell Mol Neurobiol* 30(8):1267–1274.
15. Blondel O, Bell GI, Seino S (1995) Inositol 1,4,5-trisphosphate receptors, secretory granules and secretion in endocrine and neuroendocrine cells. *Trends Neurosci* 18(4): 157–161.
16. Mitchell KJ, Lai FA, Rutter GA (2003) Ryanodine receptor type I and nicotinic acid adenine dinucleotide phosphate receptors mediate Ca^{2+} release from insulin-containing vesicles in living pancreatic beta-cells (MIN6). *J Biol Chem* 278(13): 11057–11064.
17. Putney JW, Jr. (1986) A model for receptor-regulated calcium entry. *Cell Calcium* 7(1): 1–12.
18. Cahalan MD (2009) STIMulating store-operated $Ca^{(2+)}$ entry. *Nat Cell Biol* 11(6): 669–677.
19. Hogan PG, Lewis RS, Rao A (2010) Molecular basis of calcium signaling in lymphocytes: STIM and ORAI. *Annu Rev Immunol* 28:491–533.
20. Prakriya M, et al. (2006) Orai1 is an essential pore subunit of the CRAC channel. *Nature* 443(7108):230–233.
21. Zweifach A, Lewis RS (1995) Rapid inactivation of depletion-activated calcium current (ICRAC) due to local calcium feedback. *J Gen Physiol* 105(2):209–226.
22. Malli R, Naghdi S, Romanin C, Graier WF (2008) Cytosolic Ca^{2+} prevents the subplasmalemmal clustering of STIM1: an intrinsic mechanism to avoid Ca^{2+} overload. *J Cell Sci* 121(Pt 19):3133–3139.
23. Shen WW, Frieden M, Demaurex N (2011) Local cytosolic Ca^{2+} elevations are required for stromal interaction molecule 1 (STIM1) de-oligomerization and termination of store-operated Ca^{2+} entry. *J Biol Chem* 286(42):36448–36459.
24. Palmer AE, Jin C, Reed JC, Tsien RY (2004) Bcl-2-mediated alterations in endoplasmic reticulum Ca^{2+} analyzed with an improved genetically encoded fluorescent sensor. *Proc Natl Acad Sci USA* 101(50):17404–17409.
25. Heikal AA, Hess ST, Baird GS, Tsien RY, Webb WW (2000) Molecular spectroscopy and dynamics of intrinsically fluorescent proteins: coral red (dsRed) and yellow (Citrine). *Proc Natl Acad Sci USA* 97(22):11996–12001.
26. Wuytack F, Raeymaekers L, Missiaen L (2002) Molecular physiology of the SERCA and SPCA pumps. *Cell Calcium* 32(5-6):279–305.
27. Duman JG, Chen L, Hille B (2008) Calcium transport mechanisms of PC12 cells. *J Gen Physiol* 131(4):307–323.
28. Suh BC, Lee CO, Kim KT (1995) Signal flows from two phospholipase C-linked receptors are independent in PC12 cells. *J Neurochem* 64(3):1071–1079.
29. Zitt C, et al. (2004) Potent inhibition of Ca^{2+} release-activated Ca^{2+} channels and T-lymphocyte activation by the pyrazole derivative BTP2. *J Biol Chem* 279(13): 12427–12437.
30. Park CY, et al. (2009) STIM1 clusters and activates CRAC channels via direct binding of a cytosolic domain to Orai1. *Cell* 136(5):876–890.
31. Covington ED, Wu MM, Lewis RS (2010) Essential role for the CRAC activation domain in store-dependent oligomerization of STIM1. *Mol Biol Cell* 21(11):1897–1907.
32. Duman JG, Chen L, Palmer AE, Hille B (2006) Contributions of intracellular compartments to calcium dynamics: Implicating an acidic store. *Traffic* 7(7):859–872.
33. Docampo R, de Souza W, Miranda K, Rohloff P, Moreno SN (2005) Acidocalcisomes—Conserved from bacteria to man. *Nat Rev Microbiol* 3(3):251–261.
34. Yoo SH (2011) Role of secretory granules in inositol 1,4,5-trisphosphate-dependent $Ca^{(2+)}$ signaling: From phytoplankton to mammals. *Cell Calcium* 50(2):175–183.
35. Hoogduijn MJ, et al. (2003) Melanin has a role in Ca^{2+} homeostasis in human melanocytes. *Pigment Cell Res* 16(2):127–132.
36. Christensen KA, Myers JT, Swanson JA (2002) pH-dependent regulation of lysosomal calcium in macrophages. *J Cell Sci* 115(Pt 3):599–607.
37. Quesada I, Chin WC, Steed J, Campos-Bedolla P, Verdugo P (2001) Mouse mast cell secretory granules can function as intracellular ionic oscillators. *Biophys J* 80(5): 2133–2139.
38. Quesada I, Chin WC, Verdugo P (2003) ATP-independent luminal oscillations and release of Ca^{2+} and H^{+} from mast cell secretory granules: Implications for signal transduction. *Biophys J* 85(2):963–970.
39. Yoo SH, Albanesi JP (1990) Inositol 1,4,5-trisphosphate-triggered Ca^{2+} release from bovine adrenal medullary secretory vesicles. *J Biol Chem* 265(23):13446–13448.
40. Yule DI, Ernst SA, Ohnishi H, Wojcikiewicz RJ (1997) Evidence that zymogen granules are not a physiologically relevant calcium pool. Defining the distribution of inositol 1,4,5-trisphosphate receptors in pancreatic acinar cells. *J Biol Chem* 272(14):9093–9098.
41. Zbidi H, et al. (2011) STIM1 and STIM2 are located in the acidic Ca^{2+} stores and associates with Orai1 upon depletion of the acidic stores in human platelets. *J Biol Chem* 286(14):12257–12270.
42. Lu X, Ellis-Davies GC, Levitan ES (2003) Calcium requirements for exocytosis do not delimit the releasable neuropeptide pool. *Cell Calcium* 33(4):267–271.
43. Feske S, et al. (2006) A mutation in Orai1 causes immune deficiency by abrogating CRAC channel function. *Nature* 441(7090):179–185.
44. Yang S, Zhang JJ, Huang XY (2009) Orai1 and STIM1 are critical for breast tumor cell migration and metastasis. *Cancer Cell* 15(2):124–134.
45. Zhang W, et al. (2011) Orai1-mediated I (CRAC) is essential for neointima formation after vascular injury. *Circ Res* 109(5):534–542.
46. Flourakis M, et al. (2010) Orai1 contributes to the establishment of an apoptosis-resistant phenotype in prostate cancer cells. *Cell Death Dis* 1:e75.
47. Falkenburger BH, Jensen JB, Hille B (2010) Kinetics of PIP_2 metabolism and KCNQ2/3 channel regulation studied with a voltage-sensitive phosphatase in living cells. *J Gen Physiol* 135(2):99–114.
48. Zhang B, Chenouard N, Olivo-Marin JC, Meas-Yedid V (2008) Statistical colocalization in biological imaging with false discovery control. *Biomedical Imaging: From Nano to Macro* (IEEE Conference Publications, Piscataway, NJ), pp 1327–1330.
49. Zhang Y, Chen L, Xu T (2010) Application of improved wavelet transform in biological particle detection. *Prog Biochem Biophys* 37(10):1144–1150.